Applied Thermal Engineering 178 (2020) 115445

Contents lists available at ScienceDirect

Applied Thermal Engineering

journal homepage: www.elsevier.com/locate/apthermeng

Multivariate optimization and sensitivity analyses of relevant parameters on efficiency of scraped surface heat exchanger

Ahmad Hajatzadeh Pordanjani[a], Seyed Masoud Vahedi[b], Saeed Aghakhani[c], Masoud Afrand[d,e,*], Omid Mahian[f,g], Lian-Ping Wang[h,i]

[a] Department of Mechanical Engineering, Shahrekord University, Shahrekord, Iran
[b] Department of Mechanical Engineering, Semnan University, Semnan, Iran
[c] Department of Mechanical Engineering, Najafabad Branch, Islamic Azad University, Najafabad, Iran
[d] Laboratory of Magnetism and Magnetic Materials, Advanced Institute of Materials Science, Ton Duc Thang University, Ho Chi Minh City, Vietnam
[e] Faculty of Applied Sciences, Ton Duc Thang University, Ho Chi Minh City, Vietnam
[f] School of Chemical Engineering and Technology, Xi'an Jiaotong University, Xi'an, Shaanxi 710049, China
[g] Renewable Energy and Micro/Nano Sciences Lab., Department of Mechanical Engineering, Ferdowsi University of Mashhad, Mashhad, Iran
[h] Department of Mechanics and Aerospace Engineering, Southern University of Science and Technology, Shenzhen 518055, Guangdong, China
[i] Department of Mechanical Engineering, University of Delaware, Newark, DE 19716, USA

HIGHLIGHTS

- The heat transfer rate is more affected by the rotor speed, heat flux, and mass flow rate.
- The mass flow rate and the rotor speed have the highest and the lowest impacts on the performance
- The outlet temperature is fairly independent of the rotor speed.
- Almost all optimal points happen in the highest values of rotor speed and heat flux.
- The convection heat transfer coefficient and the outlet temperature enhance by 380.64% and 4.86%.

ARTICLE INFO

Keywords:
Surface Scraped Heat Exchanger (SSHE)
Multi-Objective Optimization
Sensitivity Analysis
RNG k-ε Turbulence Model
Viscos Flow

ABSTRACT

In the current paper, a Scraped Surface Heat Exchanger (SSHE), composed of an encased rotor on which two blades are mounted, is studied. The focus is on the effects of the rotor speed, mass flow rate, and outgoing heat flux applied on the shell on the Convection Heat Transfer Coefficient (CHTC) and the Outlet Temperature (OT). To this end, the Response Surface Methodology (RSM) is utilized to achieve the regression modeling and sensitivity analysis. Then, the Nondominated Sorting Genetic Algorithm II (NSGA-II) algorithm is applied to best balance the two conflicting objectives of maximizing CHTC and minimizing OT. The results show that an increase in either the rotation speed of the rotor or mass flow rate leads to a rise in CHTC. Furthermore, decreasing the outgoing heat flux reduces CHTC and amplifies the temperature at the outlet. The sensitivity analysis indicates that OT is most sensitive to a slight change in the mass flow rate and least sensitive to change in the rotor speed. Moreover, an optimal Pareto front with 35 non-dominated optimal points is obtained.

1. Introduction

Scraped Surface Heat Exchangers (SSHEs) are a type of heat exchangers widely used in pharmaceutical, food, and chemical industries, to name a few from those listed in Fig. 1. These heat exchangers are designed for cooling or heating of fluids, especially highly viscous ones. Since increasing the size of heat exchangers brings with itself the negative consequence of increasing the pumping power, it is recommended to use smaller heat exchangers instead [1–4]. Therefore, reducing the heat transfer because of the shrinking heat exchanger has to be compensated. Using a rotor and mounting blades on it is a common approach that helps the fluid to be more agitated. As the fluid mixes, the heat transfer from the walls also increases, consequently, CHTC is improved, which is always desired for heat exchangers [5–7].

Because of their high heat transfer rate, SSHEs have attracted the attention of many researchers for many years, especially in the

* Corresponding author at: Ton Duc Thang University, Ho Chi Minh City, Vietnam.
E-mail address: masoud.afrand@tdtu.edu.vn (M. Afrand).

https://doi.org/10.1016/j.applthermaleng.2020.115445
Received 19 October 2019; Received in revised form 2 April 2020; Accepted 4 May 2020
Available online 30 May 2020
1359-4311/

Nomenclature

C_p	Specific heat,Jkg^{-1}K^{-1}
D_s	Stator diameter,m
D_r	Rotor diameter,m
H_r	Relative specific enthalpy,Jkg^{-1}
$\bar{h}$	Mean CHTC,Wm^{-2}K^{-1}
$\dot{m}$	Mass flow rate,grs^{-1}
N	Rotational speed,revs^{-1}
Nu	Nusselt number
P	Pressure,Pa
Pr	Generalized Prandtl number
$\dot{Q}_V$	Volumetric flow rate,m^{3}s^{-1}
$q_w^{"}$	Average heat flux at the casing surface,Wm^{-2}
Re	Reynolds number
T	Temperature,K
$\bar{V}$	Absolute velocity vector,ms^{-1}

Abbreviations

DoF	Degree of Freedom
F-value	Fisher test
CHTC	Convection heat transfer coefficient
MS	Mean square
OT	Outlet temperature
SS	Sum of squares

Greek letters

$\dot{\gamma}$	Shear rate,s^{-1}
δ	Clearance between tip of blade and casing,μm
λ_f	Fluid thermal conductivity,Wm^{-1}K^{-1}
ρ	Density,kgm^{-3}
ω	Rotor speed,RPM
τ	Extra stress tensor,Pa
∇	Gradient operator,m^{-1}

Subscripts and superscripts

b	Bulk
in	Inlet
o	Outlet
r	Relative
w	Wall

production of ice cream [8–12]. Blasiak and Pietriwicz [13] numerically studied the SSHE while considering the turbulence flow. Their findings demonstrated that the heat flux was between 500 and 1500 W/m^2 and CHTC varies between 20 and 45 W/m^{2}K and affected by the rotor speed. They presented a relationship for the Nusselt number, in terms of flow Reynolds and Prandtl numbers. In another study, Ali and Baccar [14] numerically examined the presence of helical ribs on the performance of a SSHE within which a Bingham fluid was flowing in steady-state, laminar condition. The positive effects of rotational speed, axial and rotational Reynolds number on the thermal performance by increasing CHTC were reported. Saraceno et al. [15] focused on how to improve the ice-cream production by SSHEs and presented two relationships for the heat transfer rate. Blasiak and Pietriwicz [16] performed a 2D simulation on a SSHE while considering the Reynolds number, Prandtl number, and the dimensionless gap in the ranges of 100 to 1000, 0.71 to 56, and 0.0005 to 0.15, respectively. Their results revealed that the increase of either Prandtl number or Reynolds number increases the heat transfer, while the increase in the dimensionless gap slightly decreases the heat transfer. Boccardi et al. [7] improved the relationships proposed for SSHEs by including the viscous dissipation effect. Comparing two different blade geometries for the rotor, Bayareh et al. [17] numerically examined the effect of blade geometry on the heat transfer of an SSHE within which pure glycerin was flowing as the working fluid. In another study, Crespí-Llorens et al. [18] studied the pressure drop and heat transfer. They examined laminar, transient, and turbulent flows and presented relationships for the Nusselt number and friction factor. Using Particle Image Velocimetry (PIV) method, Yateghene et al. [19] experimentally studied the flow pattern inside a SSHE. Their results showed that the turbulence is weak near the rotor wall, and the mixing occurred mostly alongside the rotor blades. Focusing on the flow pattern and the temperature field, Shiryan Dehkordi et al. [20] investigated the effects of blade numbers, stator length, inlet velocity,

Fig. 1. Applications of SSHEs.

fluid viscosity, the geometry of rotor blades, stator material, and rotor speed on heat transfer and OT. For the purpose of cooling down of viscous fluids, the rotor speed was found to have a positive effect on the heat transfer. Furthermore, a decrease in the stator length reduced OT so that its minimum value happens for the case of a three-blade rotor, while its maximum value happens when a single blade is mounted on the rotor. Lakhdar et al. [21] experimentally examined the heat transfer of ethylene glycol and water in a SSHE. They studied the effects of flow rate, rotor speed, and the clearance between blades and casing. Heat transfer under different conditions was investigated by many researchers [22–27]. Particle shape, particle concentration, and fluid viscosity were studied by Alhamdan and Sastry [22]. The geometry of scrapers in different axial and rotational Reynolds numbers was examined by Baccar and Abid [24]. Lee and Singh [28] studied the effects of rotor speed and flow rate of potato cubes on residence time. Harrod [27] focused on the principal design of different SSHEs. Couette flow regime and Taylor vortices regime were compared in the study of Trommelen and Beek [29].

Many studies were conducted focusing on heat transfer problems from the statistical point of view among which using Response Surface Methodology (RSM) to optimize a SSHE has many advantages over other machine-learning methods such as Artificial Neural Network (ANN) [30]. RSM is a mixed mathematical-statistical method, which provides correlations between the responses and the independent variables. Using RSM, Vahedi et al. [31] investigated the heat transfer through and over a cylinder. Two correlations were proposed for the friction factor and Nusselt number with respect to effective parameters affecting the problem. Pordanjani et al. [32,33] , Vahedi et al. [34] proposed correlations for the Nusselt number of enclosures. Proposing correlations provides an in-depth understanding of how much the output is affected by a factor. In first sight, it is very difficult to conclude that using a super-conductive fin inversely affects the heat transfer rate. RSM not only provides the initial estimates for pre-design calculations for designers also offers a broad information through regression equations and sensitivity analysis and optimization. Designers can learn from sensitivity analysis obtained from regression modeling in order to understand how much a slight change in a variable affects the response [35–37]. Pordanjani et al. [32] reported that the designer should not pay more attention to the angle between the pin fin and the hot sidewall. In fact, their sensitivity analysis showed that changing the inclination angle over a board range leads to a negligible change in the Nusselt number. Vahedi et al. [38] revealed that the thermal performance of the typical differentially-heated enclosure is not delicate to the sidewalls thickness.

According to the above survey, no study was conducted to reveal conditions leading to the best performance of a SSHE for the purpose of ice cream production. This paper not only addresses the optimization of a SSHE through which pure glycerin flows, but also the sensitivity of the outputs to the effective parameters are evaluated. The mass flow rate, rotor speed, and heat flux applied on the shell are selected as the three most effective parameters affecting the thermal performance of SSHE [20]. The lowest OT and the highest CHTC are reported, separately in single-objective optimizations and simultaneously in a two-objective optimization. Two regression modelings were also proposed for the two outputs, CHTC and OT, based on the three aforementioned factors. The results of the multi-objective optimization (the Pareto front) can provide initial ideas for designers to choose the correct avenue.

2. General description of SSHEs

Having a fully-blended and homogeneous production and at the same time providing the highest heat transfer of working fluids are the desired outcomes of industrial heat exchangers. The following types of SSHEs are promising approaches to achieve these outcomes.

2.1. Rotating, tubular dynamic SSHE

This type of SSHE consists of two coaxial cylinders. The inner cylinder is called the rotor and the outer cylinder is casing or stator. Blades, with their numbers typically varying from 1 to 4, are mounted on the rotor with the rotational speeds typically between 1 and 1000 RPM [40].

2.2. Reciprocating, tubular dynamic SSHE

This type of heat exchanger also has a similar structure to the first, but the rotor is reciprocating, with a frequency of 10 to 60 S per minute [39,40].

2.3. Rotating, plate dynamic SSHE

This type, which is highly used for cooling and heating with various rotor speeds, consists of several blades arranged in series inside a shell that clean the inner surface of the SSHE against substances [40].

As schematically depictured in Fig. 2, the first type of heat exchanger is used in the current study in which a rotor with two blades rotates to enhance the heat transfer rate and provide well-mixed, homogeneous ice cream. As shown, this type of heat exchanger comprises of two coaxial cylinders between which the working fluid flows. The fluid enters the heat exchanger from one side with a mass flow rate of $\dot{m}$ and temperature of T_{in}, swept away by the blades, and then driven to the outlet to exit with a lower temperature of T_{out}. The movement of the blades, which hinders deposition and agglomeration, is responsible for making a high-turbulent flow condition and, consequently, uniform temperature distribution.

Industrial SSHEs are generally made of stainless steel because of its availability and thermal properties, tabulated in Table 1, to achieve the desired heat transfer. The resistance against corrosion is another unique feature of stainless steel.

3. Governing equations and boundary conditions

In this work, the working fluid is Glycerin, which modeled as a Newtonian fluid with temperature-dependent viscosity. The governing equations for the steady-state, turbulent fluid flow are derived as below. Since the relative velocity is used, in the rotational frame of reference the continuity equation is given by the following equation [41,42],

$$\nabla\cdot(\rho\vec{V_{\text{r}}}) = 0 \tag{1}$$

where $\vec{V}_{\text{r}}$ is defined as

$$\vec{V_{\text{r}}} = \vec{V} - (\vec{\omega}\times\vec{r}) \tag{2}$$

where, $\vec{\omega}$ and $\vec{V}$ are the angular and absolute velocities, and $\vec{r}$ stands for the position vector of an element of fluid.

The momentum equation contains two forces of Coriolis and centrifugal; hence, the momentum equation is as follows:

$$\nabla\cdot(\rho\vec{V_{\text{r}}}\vec{V_{\text{r}}}) + \rho(2\vec{\omega}\times\vec{V_{\text{r}}} + \vec{\omega}\times\vec{\omega}\times\vec{r}) = -\nabla p + \nabla\bar{\bar{\tau}}_{\text{r}} + \rho\vec{g} \tag{3}$$

The energy equation is as follows:

$$\underbrace{\nabla\cdot\left(\rho\vec{V_{\text{r}}}H_{\text{r}}\right)}_{\text{forced heat convection}} = \underbrace{\nabla\cdot(\lambda_{\text{f}}\nabla T)}_{\text{heat conduction}} + \underbrace{\nabla\cdot\left(\bar{\bar{\tau}}_{\text{r}}\cdot\vec{V_{\text{r}}}\right)}_{\text{viscous heating}} \tag{4}$$

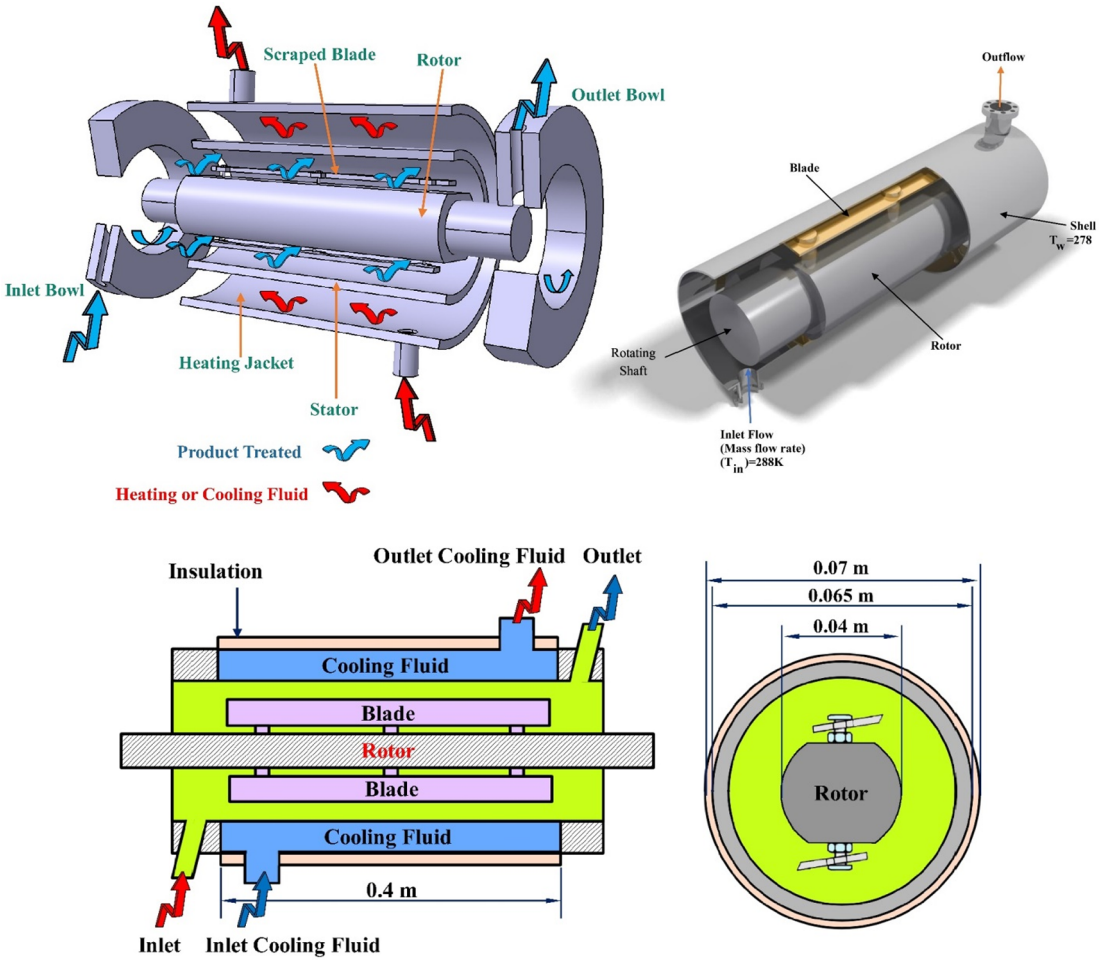

Fig. 2. A schematic view of the investigated SSHE and its dimensions.

where T is temperature, $\dot{\tau}_r(=\eta(\dot{D})\dot{D})$ is the stress tensor, and H_r is the relative total enthalpy given by the following equation.

$$H_r = E_r + \frac{p}{\rho} \tag{5}$$

where E_r is the relative internal energy which is given by the following equation.

$$E_r = h - \frac{p}{\rho} + \frac{1}{2}(V_r^2 - (\omega \times r)^2) \tag{6}$$

Viscous heating, which was appeared in Eq. (4), is considered in the current study because of the friction forces. This term can no longer be neglected in macro-scale systems when the velocity gradient or fluid viscosity is very high. The pressure and velocity gradients along the heat exchanger are high enough so that the viscous dissipation term becomes significant. Owing to the small size of the SSHE, the temperature gradient is small, thereby; slight variations in temperature significantly affects the heat transfer and any temperature-dependent properties of the fluid, particularly viscosity. For the sake of simplicity, the gravitational acceleration parameter is neglected, but the axial pressure drop is considered in the equations. The tensor of deformation rate and the shear rate are defined as follows:

$$\dot{D}_{ij} = \frac{\partial u_j}{\partial x_i} + \frac{\partial u_i}{\partial x_j} \tag{7}$$

$$|\dot{\lambda}| = \sqrt{\frac{1}{2}\dot{D}:\dot{D}} \tag{8}$$

The deformation tensor depends on the velocity gradients. For the casing of the investigated SSHE, the energy equation is as follows.

$$\nabla\cdot(\rho_m c_{pm}(-\omega \times r)T) = \nabla\cdot(\lambda_m \nabla T) \tag{9}$$

where λ_m, ρ_m, and c_{pm} are conductive heat transfer coefficient, density, and heat capacity of the stator material.

- Boundary Conditions

The rotor and its blades, which are assumed thermally insulated, rotate with a speed ranging from 100 to 500 RPM. The fluid enters at the temperature of T_{in} = 288 K and a mass flow rate of 1 to 150 g/s and

Table 1
Thermophysical properties of materials [19,41].

Material	Viscosity (Pas)	Thermal Conductivity($Wm^{-1}K^{-1}$)	Heat capacity($Jkg^{-1}K^{-1}$)	Density(kgm^{-3})
Pure glycerin	$\eta_T = 8.1.\ 10^{-12}\exp\left(\frac{7378.8}{T}\right)$	0.285	2435	1240
Stainless steel	–	16.27	502.48	8030

cools down. Passing the coolant over the stator provides a constant heat flux condition on the casing. The outgoing heat flux varies between 1000 and 4000 W/m^2. The fluid flow goes along the system while preserving the no-slip condition at solid surfaces and exits under the hydrodynamically and thermally fully developed condition [20,42].

4. Numerical modeling

4.1. Solver setting

The discretization method of momentum, energy, turbulence kinetic energy, and Reynolds stress equations was the second-order forward difference. In this method, the solution domain is comprised of a number of control volumes such that each computational cell is surrounded by control volumes without any overlapping. The SIMPLE algorithm was used to solve the discretized equations through the use of ANSYS Fluent software in a personal computer with 3.6 GHz CPU and 16 GB RAM. The solution steps are shown in Fig. 3.

4.2. Mesh independence study

In numerical studies, it is necessary to check the effect of grid resolution on the solution. Output(s) should not depend on the cells number; otherwise, the results are unreliable. As shown in Fig. 4, the geometry was meshed, non-uniformly. It is observed that the computational cells were condensed at which places where high variations in flow properties are shown, such as near the stator and the tip of blades.

The results of the mesh independence study are shown in Fig. 5. As shown, OT converges to a value, asymptotically, with increasing the number of computational cells such that no difference is seen for more than 8,765,330 cells. Thus, it was selected for the next steps.

4.3. Validation

The results of five turbulence models were compared with each other and against Ref. [41] and tabulated in Table 2. The RNG k-ε turbulence model was used for further analysis because of its lowest deviation against the experimental result of Yataghene et al. [41].

To evaluate the solution accuracy, the results of the present work should be compared against the literature. To this end, the flow and heat transfer within the SSHE whose external walls of the stator fixed at a constant temperature were compared against numerical studies of Shiryan Dehkordi et al. [20] and Yataghene et al [41]. A good agreement between these results is observable in Table 3.

5. Response Surface method

According to Dehkordi et al. [20], it has been found that many parameters affect SSHE heat transfer rate, including (1) rotor speed, (2) blade shape, (3) heat flux on the shell, (4) shell material, (5) blade number, (6) mass flow rate, and (7) length of heat exchanger. In this study, the effects of three key parameters of rotor speed, outgoing heat flux applied to the shell, and mass flow rate have been investigated. To provide a deep understanding, they have been ranked according to their influences, along with finding the best condition wherein CHTC and OT become maximum and minimum, respectively.

A hybrid statistical-mathematical method, called RSM, is used to determine the mathematical relationship between inputs and outputs [43,44]. The number of inputs and outputs can range from one to any large number. After specifying the outputs, a polynomial correlation for each output is specified in the form of the following equation:

$$Response = \alpha_0 + \sum_{i=1}^{3} \alpha_i x_i + \sum_{i=1}^{3} \alpha_{ii} x_i x_i + \sum_{i=1}^{3} \sum_{j=1, j\neq i}^{3} \alpha_{ij} x_i x_j \quad (10)$$

In the above relation, α_0, α_i, α_{ii}, and α_{ij} are unknown coefficients which will be determined by the RSM. In the first step, the effective factors along with their ranges have been specified in Table 4. Based on the face-centered central composite design method, the intervals are divided into two equal sub-intervals. The matrix of the design of experiment is obtained as in Table 5 [32,38]. As can be seen from Table 5, there are three types of factorial, axial, and central points. Columns A, B, and C present the coded values of the parameters. The values of + 1, 0, and −1, respectively, correspond to the high, middle and low levels. The corresponding real values for each parameter are listed in the three following columns of rotor speed, mass flow rate, and heat flux. After each test, the values of h and T_{out} are written within the corresponding row.

Analysis of Variance (ANOVA), [45] which was developed by statistician and evolutionary biologist Ronald Fisher, is a collection of statistical models that should be performed to evaluate the difference between numerical results and those predicted from regression modeling. Using nonlinear regression on the results of Table 5, the coefficients of Eq. (10) are obtained. Statistical tests must be passed properly

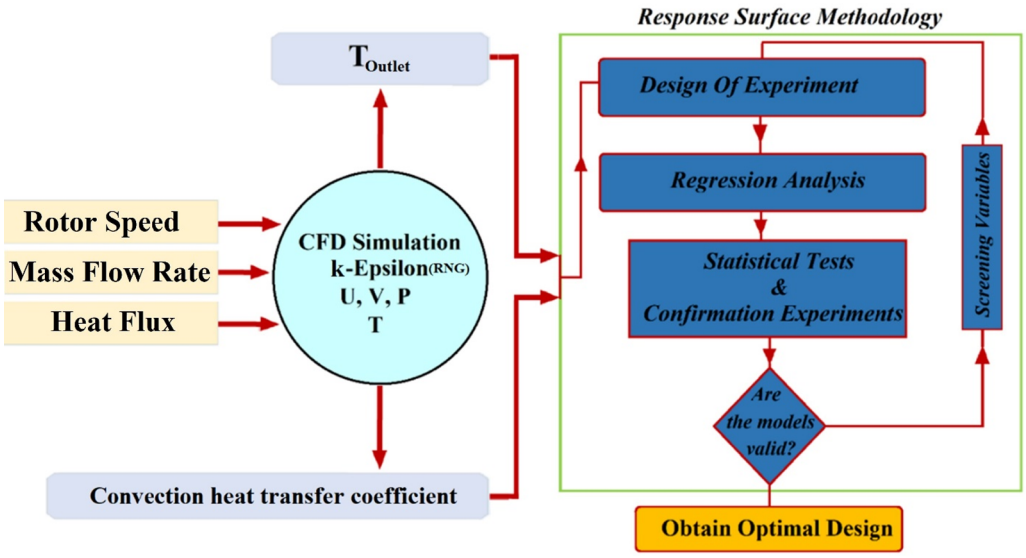

Fig. 3. A schematic representation of the solution procedure.

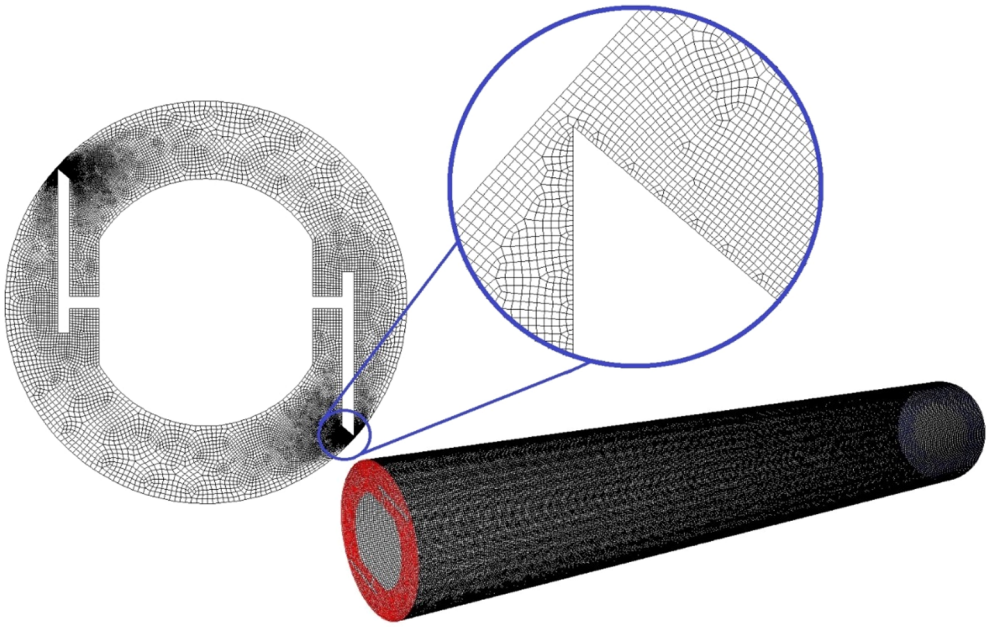

Fig. 4. A view of the generated mesh.

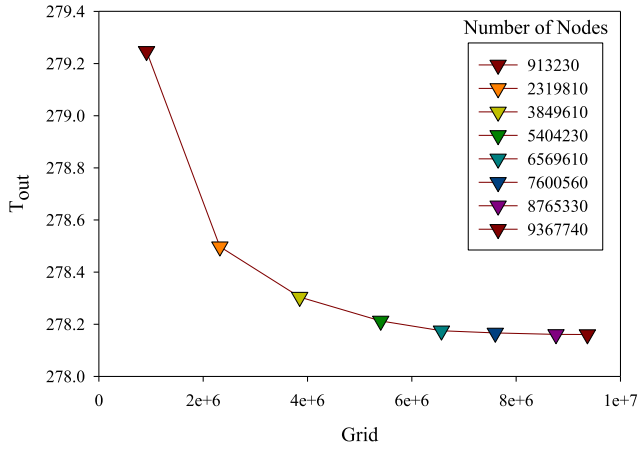

Fig. 5. Outlet temperature of the heat exchanger for different numbers of computational cells at a mass flow rate of 1.39×10^{-2}g/s.

Table 2
Assessment of different turbulence models by comparing their CHTC values at the rotor speed of 360 RPM.

Error (%)	CHTC	Model
–	384.4783	Yataghene et al. [41]
0.987	388.3109	Standard k-ε
0.195	385.2312	RNG k-ε
0.576	386.7057	Realizable k-ε
0.754	387.3992	Standard k-ω
0.232	385.3723	SST k-ω

by the established regression models to reach their most accurate correlations. ANOVA is comprised of a series of specific tests by which the accuracy of the models can be determined. SS, Dof, MS, Fisher's test (F-value), and P-value are calculated for each term to determine meaningless terms to be crossed out from the model.

ANOVA tables for the outputs have been presented in Tables 6, 7. Terms with an F-value of < 1 are excluded from the typical model of Eq. (10) [31]. Thus, as can be seen from Table 6, the term AC, which is the product of rotor speed and heat flux, is crossed out from the

Table 3
A comparison of CHTC between the present work and the literature.

Rotor speed	Present work	Ref. [20]	Ref. [41]	%Error Ref. [20]	Ref. [41]
120	290.3430	297.9630	288.3211	2.553%	0.696%
240	351.8654	352.0870	351.4323	0.062%	0.123%
360	385.2312	385.3680	384.4783	0.035%	0.195%
480	401.9856	401.8940	403.5432	0.022%	0.385%
600	412.0765	413.0700	411.7843	0.240%	0.070%

Table 4
Three selected parameters along with their intervals.

Variable	Actual parameter	Coded symbol	Levels Low (-1)	Mid (0)	High (+1)
Rotor speed(RPM)	ω	A	100	300	500
Mass flow rate(gr. s^{-1})	$\dot{m}$	B	1	75.5	150
Heat flux(Wm^{-2})	$q^{"}$	C	1000	2500	4000

regression model of $h^{0.41}$. Also, the regression model of T_{out}^3 is independent of $\omega\dot{m}$, ω^2, $\omega q_w^{"}$, and $q_w^{"2}$. In this way, the regression equations are reduced and become simpler and more predictable.

Tables 8 and 9 are the modifications of Tables 6 and 7, respectively. It can be seen that all terms are meaningful and have good statistical indices. Finally, the parameters of R^2 and adjusted-R^2, which indicate the uncertainty of the models, are the most important indices for evaluating the predictability of the models [46,47].

$$R^2 = 1 - \frac{SS_E}{SS_T} \tag{11}$$

$$R^2_{adj} = 1 - \frac{\frac{SS_E}{(n-p)}}{\frac{SS_T}{(n-p)}} = 1 - \frac{n-1}{n-p}(1-R^2) \tag{12}$$

The values of R^2 and adjusted-R^2 are, respectively, 0.9994 and 0.9985 for CHTC and 0.9882 and 0.9816 for OT. This means that the models with the values of 1% and 2% have predictive power, respectively.

Table 5
Design matrix of tests based on the central composite design method.

Run number	Point type	Coded values			Real values			Responses	
		A	B	C	Rotor speed	Mass flow rate	Heat flux	h	T_{out}
1	Factorial	−1	−1	−1	100	1	1000	128.84	280.58
2		−1	−1	+1	100	1	4000	243.62	273.26
3		−1	+1	−1	100	150	1000	353.17	286.67
4		−1	+1	+1	100	150	4000	458.43	285.85
5		+1	−1	−1	500	1	1000	147.5	281.7
6		+1	−1	+1	500	1	4000	274.7	274.59
7		+1	+1	−1	500	150	1000	475.49	286.97
8		+1	+1	+1	500	150	4000	596.56	286.32
9	Axial	−1	0	0	100	75.5	2500	400	285.18
10		0	−1	0	300	1	2500	224.66	277.94
11		0	0	−1	300	75.5	1000	367.32	285.98
12		0	0	+1	300	75.5	4000	507.86	284.81
13		0	+1	0	300	150	2500	527.94	286.5
14		+1	0	0	500	75.5	2500	505.99	285.6
15	Center	0	0	0	300	75.5	2500	470.79	285.39

5.1. Presentation of models and diagnostic tests

The established models could be trusted after statistical evaluations. It should be noted that these models are valid in the ranges of $100 < \omega(\mathrm{RPM}) < 500$, $1 < \dot{m}(\mathrm{gr.\ S^{-1}}) < 150$, and $1000 < q''(\mathrm{Wm^{-2}}) < 4000$.

$$h^{0.41} = 5.40822 + 0.004345\omega + 0.062038\dot{m} + 0.001618q_w'' + 16 \times 10^{-6}\omega \cdot\dot{m} - 2.19979 \times 10^{-6}\dot{m}\cdot q_w'' - 5.19341 \times 10^{-6}\omega^2 - 238 \times 10^{-6}\dot{m}^2 - 1.77 \times 10^{-7}q_w''^2 \quad (13)$$

$$T_{out}^3 = 2.25318 \times 10^7 + 428.51375\omega + 27265.322\dot{m} - 516.51q_w'' + 3.325\dot{m} \cdot q_w'' - 142.15\dot{m}^2 \quad (14)$$

The predictability of the models is depicted in Figs. 6, 7, visually. These figures include the normal distribution and a scatter plot of the predicted values against the actual values extracted from the code. The closer the pattern of scatters to the line results in a higher accuracy of the model [48,49]. As can be observed, the normal distribution of both CHTC and OT follow this condition. In these figures, furthermore, the values obtained from the regression models have been also plotted versus their actual values. Distribution of scatters being closer to the 45° bisector means that the models have high accuracy in predicting the design points [49].

5.2. Response surfaces

Fig. 8 demonstrates 3D surfaces and 2D contours of the averaged CHTC. In each figure, two variables vary in their investigated ranges, while the third variable is fixed at its middle level. As can be seen, mass flow rate, rotor speed, and the heat flux from the casing of the SSHE have favorable effects on CHTC. It is also observed that the effect of mass flow rate on CHTC is greater than that of the other two parameters. For the case of fixed cross-section, the fluid velocity rises with flow rate according to the mass conservation law. Increasing fluid velocity also raises the temperature gradient and CHTC, as well. The higher the turbulent flow, the higher the heat transfer rate. Accordingly, increasing the rotor speed causes more fluid mixing and higher convection heat transfer. The reason for the positive effect of heat flux is that the heat transfer from the stator shell is in direct relation with the applied heat flux.

Fig. 9 depicts 3D surfaces and 2D contours of OT as a function of other variables. As can be seen, OT always increases with increasing rotor speed and the mass flow rate and always decreases with increasing the heat flux imposed on the shell. Raising the flow rate causes the fluid to flow with higher velocity and insufficient time to extract heat, resulting in a rise of OT. Increasing the outward heat flux from 1000 W/m^2 to 4000 W/m^2 raises the fluid-to-wall heat transfer rate, eventually leading to a decrease in OT. As mentioned before, the heat transfer increases with rotor speed expecting the reduction of OT. While Fig. 9 shows that something different happens. Although increasing heat transfer is associated with reducing the fluid temperature

Table 6
ANOVA outputs for h.

Source	SS	DOF	MS	F-value	P-value	
Model	55.39	9	6.15	882.	< 0.0001	
ω	2.42	1	2.42	347.34	< 0.0001	
$\dot{m}$	35.9	1	35.9	5146.84	< 0.0001	
q_w''	7.24	1	7.24	1038.18	< 0.0001	
$\omega\dot{m}$	0.4731	1	0.4731	67.83	0.0004	
$\omega q_w''$	0.001	1	0.001	0.0178	0.8991	Not Significant
$\dot{m}q_w''$	0.4834	1	0.4834	69.31	0.0004	
ω^2	0.111	1	0.111	15.91	0.0104	
$\dot{m}^2$	4.5	1	4.5	645.62	< 0.0001	
$q_w''^2$	0.4079	1	0.4079	58.49	0.0006	
Residual	0.0349	5	0.007			
R^2 = 99.94%			**Standard Deviation**= 0.058			
Adjusted R^2 = 99.82%			**Mean**= 1.66			
Predicted R^2 = 99.41%			**C.V. %**= 3.51			
Adequate Precision= 94.9651						

Table 7
ANOVA outputs for T_{out}.

Source	SS	DOF	MS	F-value	P-value	
Model	1.591×10^{13}	9	1.768×10^{12}	52.52	0.0002	
ω	7.345×10^{10}	1	7.345×10^{10}	2.18	0.1997	
$\dot{m}$	1.105×10^{13}	1	1.105×10^{13}	328.35	< 0.0001	
q_w''	1.586×10^{12}	1	1.586×10^{12}	47.1	0.001	
$\omega\dot{m}$	1.763×10^{10}	1	1.763×10^{10}	0.5236	0.5017	Not Significant
$\omega q_w''$	7.065×10^{8}	1	7.065×10^{8}	0.0210	0.8905	Not Significant
$\dot{m}q_w''$	1.105×10^{12}	1	1.105×10^{12}	32.81	0.0023	
ω^2	1.210×10^{9}	1	1.210×10^{9}	0.0360	0.8571	Not Significant
$\dot{m}^2$	1.533×10^{12}	1	1.533×10^{12}	45.55	0.0011	
$q_w''^2$	1.051×10^{9}	1	1.051×10^{9}	0.0312	0.8667	Not Significant
Residual	1.683×10^{11}	5	3.367×10^{10}			
R^2 = 98.95%			**Standard Deviation**= 1.835×10^{5}			
Adjusted R^2 = 97.07%			**Mean**= 2.272×10^{7}			
Predicted R^2 = 90.68%			**C.V. %**= 0.8076			
Adequate Precision= 21.0615						

Table 8
ANOVA outputs for $h^{0.41}$.

Source	SS	DOF	MS	F-value	P-value
Model	55.39	8	6.92	1186.94	< 0.0001
A-ω	2.42	1	2.42	415.33	< 0.0001
B-$\dot{m}$	35.9	1	35.9	6154.30	< 0.0001
C-q_w''	7.24	1	7.24	1241.39	< 0.0001
AB	0.4731	1	0.4731	81.11	< 0.0001
BC	0.4834	1	0.4834	82.88	< 0.0001
A^2	0.111	1	0.111	19.02	0.0048
B^2	4.5	1	4.5	771.99	< 0.0001
C^2	0.4079	1	0.4079	69.93	0.0002
Residual	0.0350	6	0.0058		
R^2 = 99.94%			**Standard Deviation**= 0.0764		
Adjusted R^2 = 99.85%			**Mean**= 11.18		
Predicted R^2 = 99.62%			**C.V. %**= 0.6833		
Adequate Precision = 109.4615					

everywhere in the heat exchanger, the heat generation because of the viscous dissipation is amplified by increasing rotor speed so that the later effect becomes dominant resulting in a slight rise of temperature. As a matter of fact, the two factors produce opposite effects on OT. By and large, the slight dependence of OT upon rotor speed is evident in the figures indicating that the positive effect of extracting heat and the negative effect of viscous dissipation are comparable. Thus, the lowest value of OT corresponds to the highest heat flux applied on the shell, and the lowest values of rotor speed and flow rate.

5.3. Sensitivity analysis

Sensitivity analysis measures the variations of independent parameters with a slight change in variables. The length of bars means the intensity of variations, positive/negative bar stands for a direct/inverse relationship [51]. Figs. 10 and 11 demonstrate the sensitivities of CHTC and OT to the three factors. Factor A is set to its central value (the coded value of 0) at 300 RPM. Then, the sensitivity of the responses to slight variations of variables is observed by changing the factor B (mass flow rate) and C (heat flux). As shown in Fig. 10, CHTC always increases with increasing rotor speed. But, its behavior is slightly different for the mass flow rate and heat flux. In fact, CHTC is in direct relation to the mass flow rate (B) at its low and medium values, but at its high value, this trend is reversed.

Fig. 11 displays the sensitivity of OT to the factors. As can be seen, the outlet temperature has the lowest sensitivity to rotor speed and the highest sensitivity to the flow rate. However, the latter one is slightly more complicated such that at its low and middle levels, the temperature increases with a slight change in $\dot{m}$, while this trend is reversed in its high value.

5.4. Optimization

Finally, after analyzing the behavior of responses, an optimization is performed to achieve the best result. Using optimization, input values can be found in a way that a specific goal is obtained. From the industrial point of view, designers always seek for the best set of input

Table 9
ANOVA outputs for T_{out}^3.

Source	SS	DOF	MS	F-value	P-value
Model	1.589×10^{13}	5	3.179×10^{12}	150.70	< 0.0001
A-ω	7.345×10^{10}	1	7.345×10^{10}	3.48	0.0949
B-$\dot{m}$	1.105×10^{13}	1	1.105×10^{13}	524.09	< 0.0001
C-q_w''	1.586×10^{12}	1	1.586×10^{12}	75.18	< 0.0001
BC	1.105×10^{12}	1	1.105×10^{12}	52.36	< 0.0001
B^2	2.075×10^{12}	1	2.075×10^{12}	98.37	< 0.0001
Residual	1.898×10^{11}	9	2.109×10^{10}		
R^2 = 98.82%			**Standard Deviation**= 1.452×10^{5}		
Adjusted R^2 = 98.16%			**Mean**= 2.272×10^{7}		
Predicted R^2 = 96.82%			**C.V. %**= 0.6393		
Adequate Precision = 33.6849					

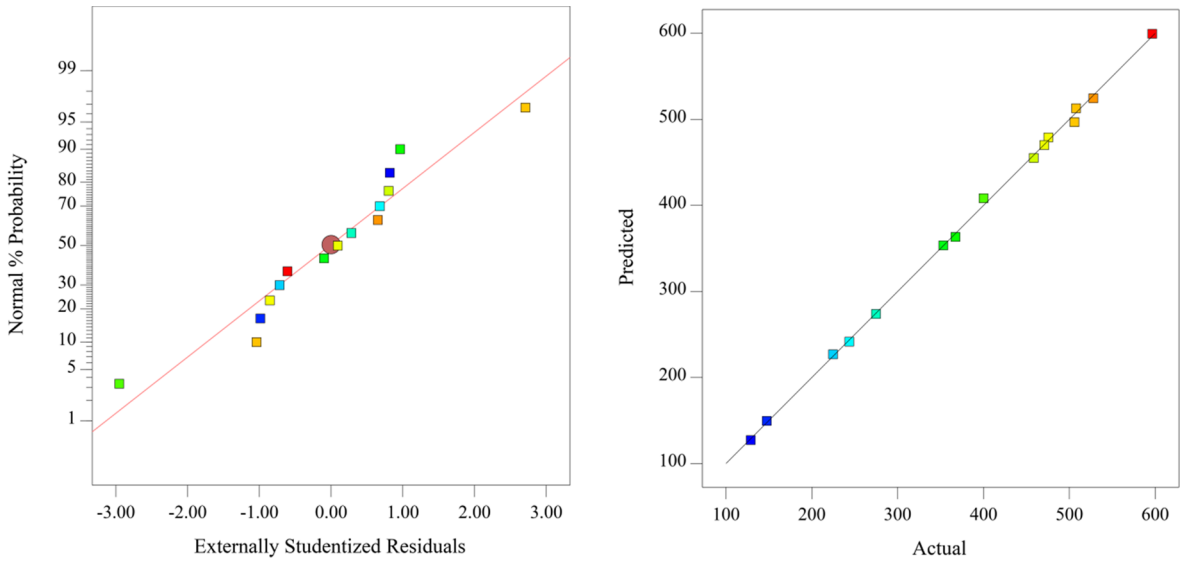

Fig. 6. The normal distribution (left) and the drawing of the predicted values against the actual values (right) of $h^{0.41}$.

values to reach production. The purpose of optimization is usually to maximize or minimize responses, individually or simultaneously. SSHEs show their best performance when the temperature difference between the inlet and outlet is increased as much as it can be. In the first stage, a deeper understanding of the results is provided by individually optimizing the responses and figuring out the minimum and maximum reachable values of the responses. Thus, firstly, two single-objective optimizations are performed to find the minimum OT and the maximum CHTC, separately. Afterward, a two-objective optimization is performed to reach the aforementioned objectives, simultaneously.

- ***Single-objective optimization***

In this stage, one response is optimized disregarding other available response(s). In the present work, the optimum points are obtained through the use of the hill-climbing technique. The hill-climbing technique, like as Monte-Carlo, simulated annealing, and genetic algorithms, is a greedy search engine seeking for the best solution of a specified function. A random starting point is selected first, and then the algorithm evaluates adjacent points to check whether it is better or not. In fact, it is a gradient-based technique in which the output strongly depends on the initial guess. One of the deficiencies of the method is finding a local optimum solution, while probable better solutions exist in other zones. To overcome the problem, and to ensure that all peaks are reachable, the number of random restart points should be large, at least larger than the number of peak points. Unfortunately, predicting the zones wherein optimum solutions happen is almost impossible, even for simple problems, one should set a large value for the random restart setting. CHTC and OT are introduced, respectively, as a hill and a hollow from which the maximum and the minimum must be found. As shown in Fig. 12, the maximum CHTC is 611.703W/m^2 happened at 500RPM, 150g/m^3, 4000W/m^2 and the minimum of OT happened at 100.012RPM, 1.001g/m^3, 3998.57W/m^2, distinctly.

- ***Multi-objective optimization***

In a multi-objective optimization in which more than one goal was defined, sometimes finding the optimal solution is not possible without using the optimization algorithms. For the problems with conflicting

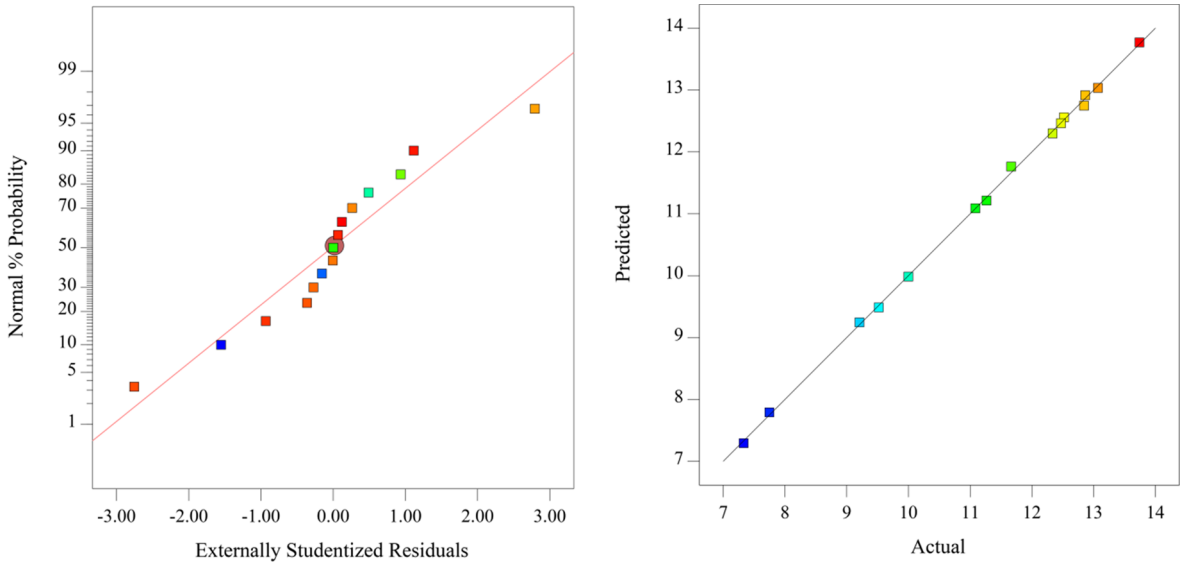

Fig. 7. The normal distribution (left) and the drawing of the predicted values against the actual values (right) of T_{out}^3.

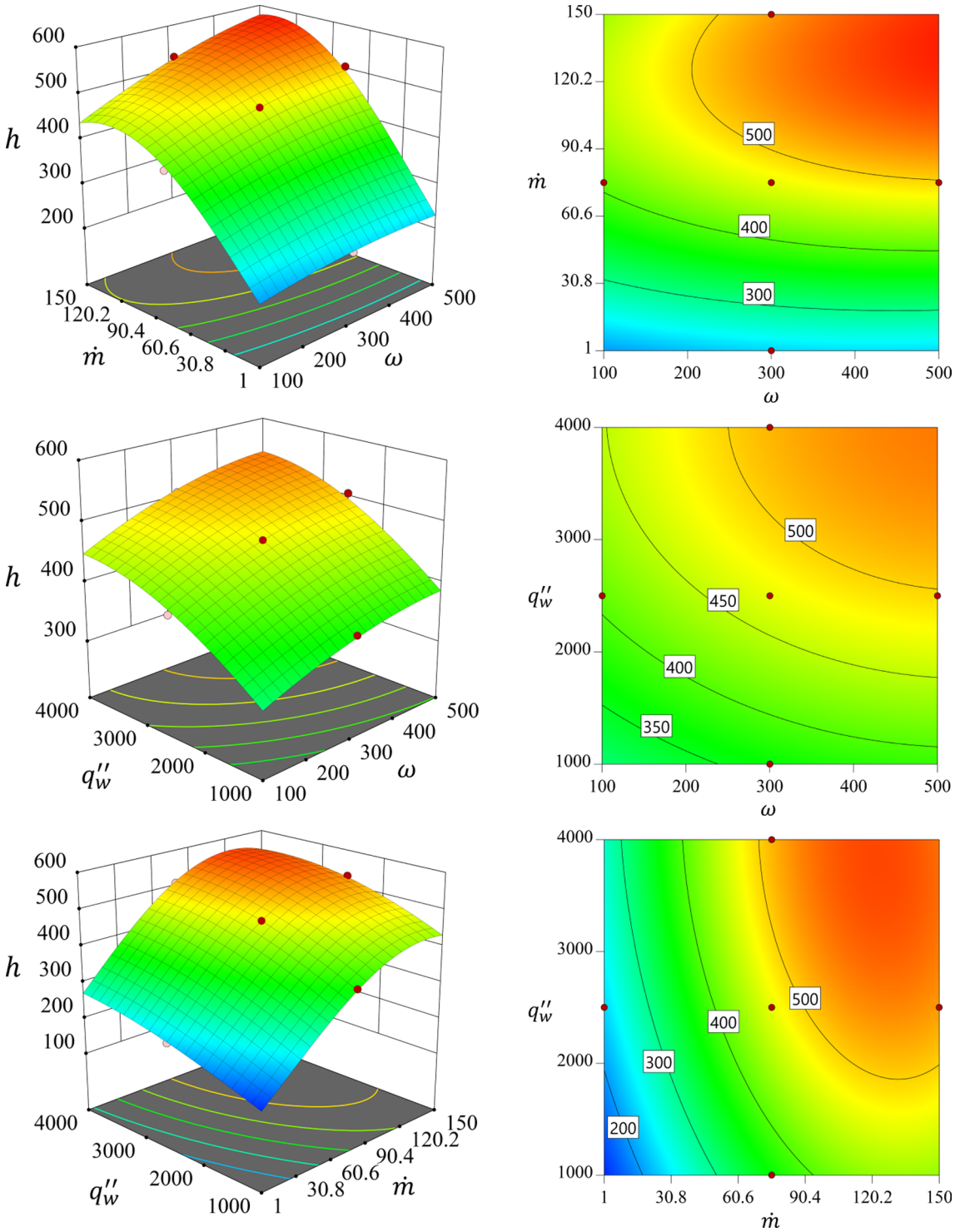

Fig. 8. Variations of CHTC as a 3D surface and a 2D contour with respect to (a) mass flow rate and rotor speed, (b) rotor speed and heat flux, and (c) heat flux and mass flow rate.

objectives, reaching a better solution for an objection may result in a worse solution for others. For such problems, a set of optimal points is obtained and designers have to make a trade-off. In the current problem, the best solution would be the one with the highest heat transfers while OT reaches its minimum value, namely, reaching the highest value for h and the minimum T_{out}. The response surface plots and sensitivity analysis reveal that it is not possible to have both of the goals, simultaneously. The Nondominated Sorting Genetic Algorithm II (NSGA-II) has been employed to overcome the problem. The method needs an initial set of population, which is randomly selected, to start. Then, based on the objective functions and domination concept, the initial population sorted in a number of Pareto fronts. Fronts are ranked based on the domination concept. Points on the same Pareto front have no superiority over each other. To avoid crowding the solutions in a local region, the crowding distance operator has been used, through which the optimal points of a special front are placed, fairly, in equal distance from each other. In the next step, using binary tournament and based on the value of crowding distance and non-domination rank, the

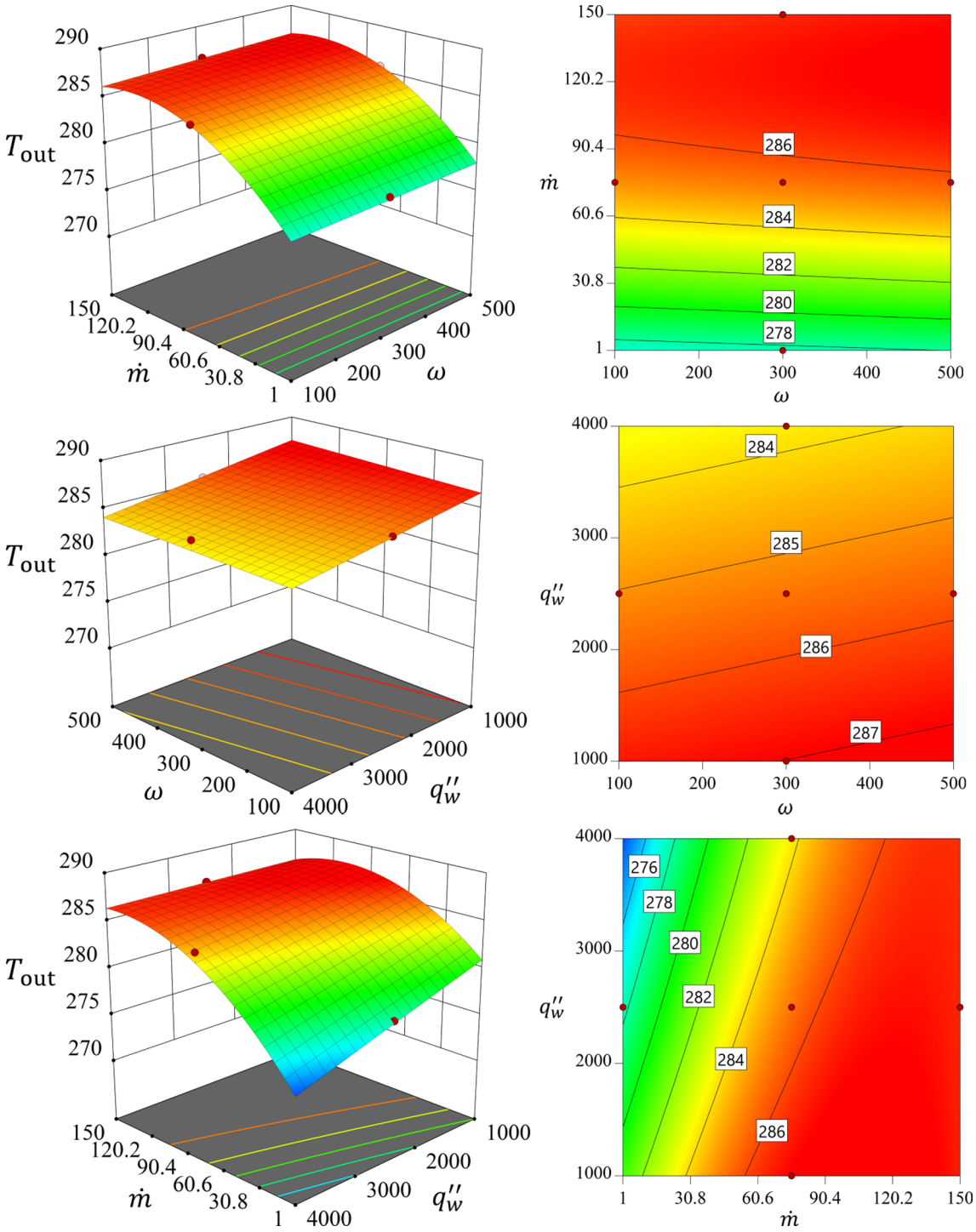

Fig. 9. Variations of the temperature as a 3D surface and a 2D contour with respect to (a) mass flow rate and rotor speed, (b) rotor speed and heat flux, and (c) heat flux and mass flow rate.

parent population is selected. Consequently, the offspring population would be generated. Elites are preserved for the next generation from all of the points of the two populations. Fig. 12 shows the 1st, 8th, 20th, 30th, and the optimal Pareto front. The x- and y-axis are CHTC and OT, respectively. After more than 35 iterations, the solution is converged and the Pareto front does not significantly change. It can be seen from the scatters that the crowding distance has taken into account. Optimal points on the Pareto fronts are non-dominated capable of meeting a designer's condition. It is worth noting that h enhances by 380.64% along the Pareto front, while OT enhances by about 4.86%, which shows that the h varies strongly along the optimal points and depends strongly on the selection.

The Pareto fronts are sorted according to the increase of CHTC and plotted in Fig. 13. It is interesting to note that all of the optimal points happen at rotor speed and heat flux of 500(RPM) and 4000(W/m^2). In fact, for the application in which OT is more important than CHTC, $\dot{m}$ must be set to its lowest value. In fact, it plays the most important role in changing the optimal points and makes the objectives conflicting. The abrupt change between the fourth and the fifth optimal points happens for the rotor speed again implies the low sensitivity of the

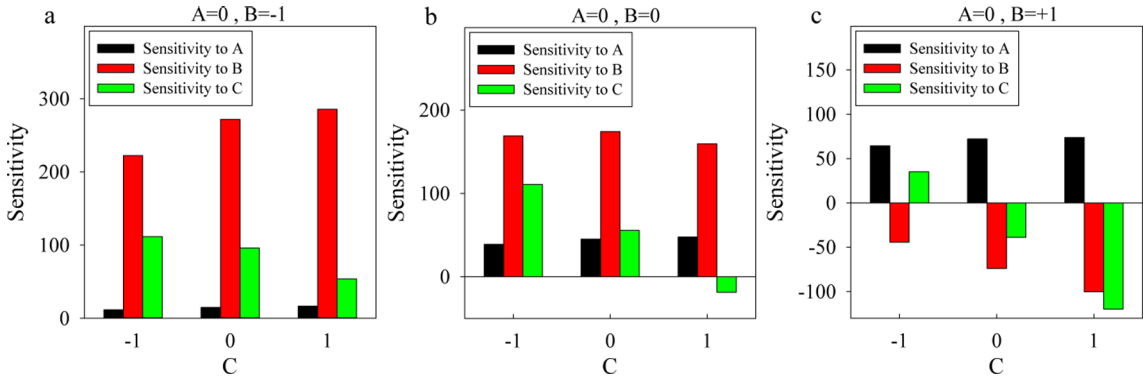

Fig. 10. Sensitivity of CHTC to the factors.

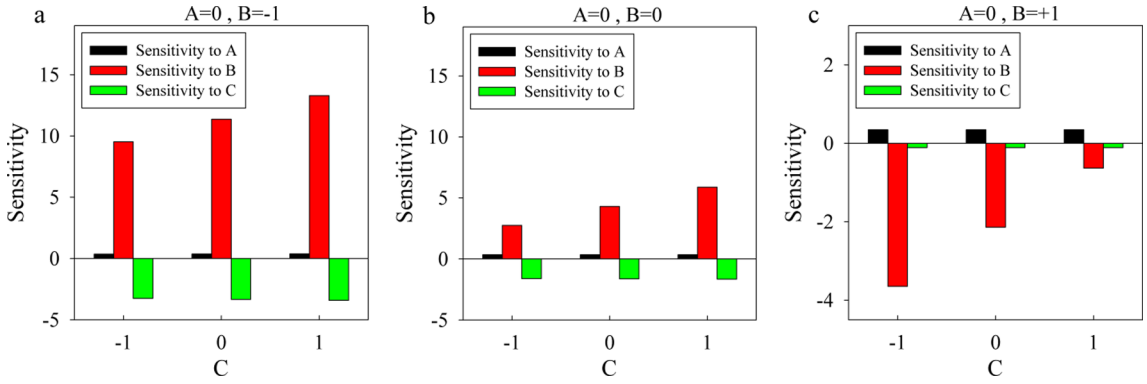

Fig. 11. Sensitivity of OT to the factors.

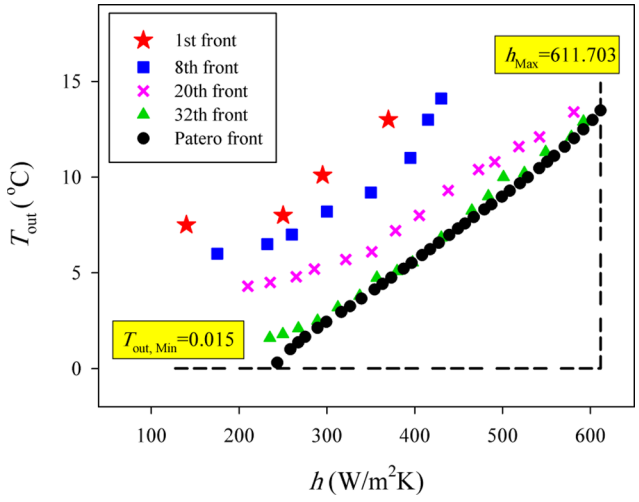

Fig. 12. The optimal points on the Pareto front with the highest CHTC and the lowest OT resulted from single-objective optimization.

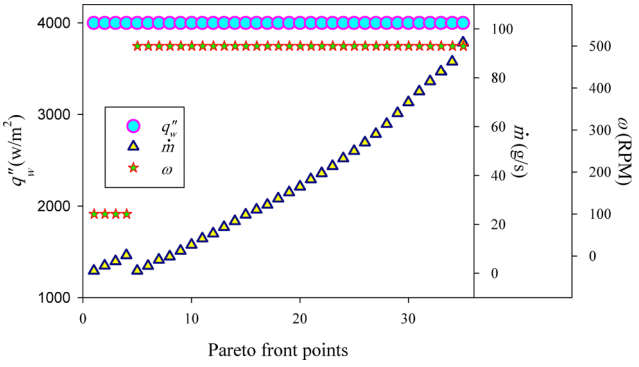

Fig. 13. Input values for all of the 35 optimal points.

optimal points on the rotor speed. In fact, the insignificant influence of the rotor speed is reflected in the abrupt change such that increasing the rotor speed from its lowest to its highest values provides no significant reduction in OT. Thus, from the electrical energy saving point of view, if the purpose is reaching the lowest OT the rotor speed should be set to its lowest value, namely 100RPM.

5.5. Conclusion

The performance of a Surface Scraped Heat Exchanger is investigated in this paper by numerical modeling. This type of heat exchanger is used for heat transfer of highly viscous fluids in many industries. The simulated heat exchanger comprises a stator and a rotor on which two blades are designed to blend the fluid at a constant speed. The fluid enters the heat exchanger steadily with constant mass flow rate and temperature and then cools down. The effects of three key parameters of rotor speed, flow rate, and the heat flux imposed on the casing, on the outlet temperature and the convection heat transfer coefficient are examined. Finally, the values of these parameters are optimized to maximize the convection heat transfer coefficient and minimize the outlet temperature. The results are summarized as follows:

- Increasing the rotor speed has favorable and unfavorable effects on the convection heat transfer coefficient and the outlet temperature.
- At low and middle levels of mass flow rate, increasing its value raises the convection heat transfer coefficient, but this also causes the unfavorable increase in the outlet temperature. Such a trend is observed in a high level of mass flow rate but in the inverse direction.

- The outlet temperature of the heat exchanger is least sensitive to the rotor speed and is most sensitive to the mass flow rate.
- Maximizing the convection heat transfer coefficient and minimizing the outlet temperature are conflicting objectives, thus the results of optimization are provided as a set of non-dominated optimal solutions.
- The convection heat transfer coefficient enhances by 380.64% along the Pareto front, while the outlet temperature enhances by 4.86%, which shows that the convection heat transfer coefficient highly depends on the selection of optimal points.

Declaration of Competing Interest

The authors declared that there is no conflict of interest.

References

[1] L. D'Addio, C. Carotenuto, F. Di Natale, R. Nigro, A new arrangement of blades in scraped surface heat exchangers for food pastes, J. Food Eng. 108 (2012) 143–149.
[2] A. Hajatzadeh Pordanjani, S. Aghakhani, M. Afrand, B. Mahmoudi, O. Mahian, S. Wongwises, An updated review on application of nanofluids in heat exchangers for saving energy, Energy Convers. Manage. 198 (2019) 111886.
[3] R.W. Hartel, Ice crystallization during the manufacture of ice cream, Trends Food Sci. Technol. 7 (1996) 315–321.
[4] A. Russell, P. Cheney, S. Wantling, Influence of freezing conditions on ice crystallisation in ice cream, J. Food Eng. 39 (1999) 179–191.
[5] A. Maxson, L. Watson, P. Karandikar, J. Zakin, Heat transfer enhancement in turbulent drag reducing surfactant solutions by agitated heat exchangers, Int. J. Heat Mass Transf. 109 (2017) 1044–1051.
[6] A. Maxson, Heat Transfer Enhancement in Turbulent Drag Reducing Surfactant Solutions, in, The Ohio, State University, 2017.
[7] G. Boccardi, G. Celata, R. Lazzarini, L. Saraceno, R. Trinchieri, Development of a heat transfer correlation for a scraped-surface heat exchanger, Appl. Therm. Eng. 30 (2010) 1101–1106.
[8] F. Bozzoli, S. Rainieri, M. Mordacci, G. Pagliarini, Experimental investigation on the heat transfer performance of a scraped surface heat exchanger for highly viscous foods, in: 2010 14th International Heat Transfer Conference, American Society of Mechanical Engineers Digital Collection, 2010, pp. 713-718.
[9] K.-H. Sun, D. Pyle, A. Fitt, C. Please, M.J. Baines, N. Hall-Taylor, Numerical study of 2D heat transfer in a scraped surface heat exchanger, Comput. Fluids 33 (2004) 869–880.
[10] M. Stranzinger, K. Feigl, E. Windhab, Non-Newtonian flow behaviour in narrow annular gap reactors, Chem. Eng. Sci. 56 (2001) 3347–3363.
[11] E. Dumont, F. Fayolle, J. Legrand, Flow regimes and wall shear rates determination within a scraped surface heat exchanger, J. Food Eng. 45 (2000) 195–207.
[12] E. Dumont, F. Fayolle, J. Legrand, Electrodiffusional wall shear rate analysis in scraped surface heat exchanger, AIChE J. 46 (2000) 1138–1148.
[13] P. Błasiak, S. Pietrowicz, An experimental study on the heat transfer performance in a batch scraped surface heat exchanger under a turbulent flow regime, Int. J. Heat Mass Transf. 107 (2017) 379–390.
[14] S. Ali, M. Baccar, Numerical study of hydrodynamic and thermal behaviors in a scraped surface heat exchanger with helical ribbons, Appl. Therm. Eng. 111 (2017) 1069–1082.
[15] L. Saraceno, G. Boccardi, G. Celata, R. Lazzarini, R. Trinchieri, Development of two heat transfer correlations for a scraped surface heat exchanger in an ice-cream machine, Appl. Therm. Eng. 31 (2011) 4106–4112.
[16] P. Błasiak, S. Pietrowicz, Towards a better understanding of 2D thermal-flow processes in a scraped surface heat exchanger, Int. J. Heat Mass Transf. 98 (2016) 240–256.
[17] M. Bayareh, A.H. Pordanjani, A.A. Nadooshan, K.S. Dehkordi, Numerical study of the effects of stator boundary conditions and blade geometry on the efficiency of a scraped surface heat exchanger, Appl. Therm. Eng. 113 (2017) 1426–1436.
[18] D. Crespí-Llorens, P. Vicente, A. Viedma, Experimental study of heat transfer to non-Newtonian fluids inside a scraped surface heat exchanger using a generalization method, Int. J. Heat Mass Transf. 118 (2018) 75–87.
[19] M. Yataghene, F. Francine, L. Jack, Flow patterns analysis using experimental PIV technique inside scraped surface heat exchanger in continuous flow condition, Appl. Therm. Eng. 31 (2011) 2855–2868.
[20] K.S. Dehkordi, M.A. Fazilati, A. Hajatzadeh, Surface scraped heat exchanger for cooling newtonian fluids and enhancing its heat transfer characteristics, a review and a numerical approach, Appl. Therm. Eng. 87 (2015) 56–65.
[21] M.B. Lakhdar, R. Cerecero, G. Alvarez, J. Guilpart, D. Flick, A. Lallemand, Heat transfer with freezing in a scraped surface heat exchanger, Appl. Therm. Eng. 25 (2005) 45–60.
[22] A. Alhamdan, S. Sastry, Residence time distribution of food and simulated particles in a holding tube, J. Food Eng. 34 (1997) 271–292.
[23] A. Alhamdan, S.K. Sastry, Residence time distribution of food and simulated particles in a model horizontal swept surface heat exchanger 1, J. Food Process Eng., 21 (1998) 145-180.
[24] M. Baccar, M.S. Abid, Numerical analysis of three-dimensional flow and thermal behaviour in a scraped-surface heat exchanger, Revue générale de thermique 36 (1997) 782–790.
[25] D. Chandarana, J. Unverferth, Residence time distribution of particulate foods at aseptic processing temperatures, J. Food Eng. 28 (1996) 349–360.
[26] H. Khartabil, R. Christensen, An improved scheme for determining heat transfer correlations from heat exchanger regression models with three unknowns, Exp. Therm Fluid Sci. 5 (1992) 808–819.
[27] M. Härröd, Scraped surface heat exchangers: a literature survey of flow patterns, mixing effects, residence time distribution, heat transfer and power requirements, J. Food Process Eng 9 (1986) 1–62.
[28] J.H. Lee, R.K. Singh, Residence time distribution characteristics of particle flow in a vertical scraped surface heat exchanger, J. Food Eng. 18 (1993) 413–424.
[29] A. Trommelen, W. Beek, Flow phenomena in a scraped-surface heat exchanger ("Votator"-type), Chem. Eng. Sci. 26 (1971) 1933–1942.
[30] K.M. Desai, S.A. Survase, P.S. Saudagar, S. Lele, R.S. Singhal, Comparison of artificial neural network (ANN) and response surface methodology (RSM) in fermentation media optimization: case study of fermentative production of scleroglucan, Biochem. Eng. J. 41 (2008) 266–273.
[31] S.M. Vahedi, A.H. Pordanjani, A. Raisi, A.J. Chamkha, Sensitivity analysis and optimization of MHD forced convection of a Cu-water nanofluid flow past a wedge, European Phys. J. Plus 134 (2019) 124.
[32] A.H. Pordanjani, S.M. Vahedi, F. Rikhtegar, S. Wongwises, Optimization and sensitivity analysis of magneto-hydrodynamic natural convection nanofluid flow inside a square enclosure using response surface methodology, J. Therm. Anal. Calorim. 135 (2019) 1031–1045.
[33] A.H. Pordanjani, S.M. Vahedi, S. Aghakhani, M. Afrand, H.F. Öztop, N. Abu-Hamdeh, Effect of magnetic field on mixed convection and entropy generation of hybrid nanofluid in an inclined enclosure: Sensitivity analysis and optimization, Europ. Phys. J. Plus 134 (2019) 412.
[34] S.M. Vahedi, A.H. Pordanjani, S. Wongwises, M. Afrand, On the role of enclosure side walls thickness and heater geometry in heat transfer enhancement of water–Al2O3 nanofluid in presence of a magnetic field, J. Therm. Anal. Calorim. 138 (2019) 679–696.
[35] M. Rejvani, A. Alipour, S.M. Vahedi, A.J. Chamkha, S. Wongwises, Optimal characteristics and heat transfer efficiency of SiO2/water nanofluid for application of energy devices: a comprehensive study, Int. J. Energy Res. 43 (2019) 8548–8571.
[36] M. Rejvani, S. Saedodin, S.M. Vahedi, S. Wongwises, A.J. Chamkha, Experimental investigation of hybrid nano-lubricant for rheological and thermal engineering applications, J. Therm. Anal. Calorim. 138 (2019) 1823–1839.
[37] R. Zhang, S. Aghakhani, A.H. Pordanjani, S.M. Vahedi, A. Shahsavar, M. Afrand, Investigation of the entropy generation during natural convection of Newtonian and non-Newtonian fluids inside the L-shaped cavity subjected to magnetic field: application of lattice Boltzmann method, Europ. Phys. J. Plus 135 (2020) 184.
[38] S.M. Vahedi, A.H. Pordanjani, S. Wongwises, M. Afrand, On the role of enclosure side walls thickness and heater geometry in heat transfer enhancement of water–Al_2O_3 nanofluid in presence of a magnetic field, J. Therm. Anal. Calorim. 138 (2019) 679–696.
[39] R. De Goede, E. De Jong, Heat transfer properties of a scraped-surface heat exchanger in the turbulent flow regime, Chem. Eng. Sci. 48 (1993) 1393–1404.
[40] R.L. Smith, C.C. Yann, Dual scraped surface heat exchanger, in, Google Patents, 1978.
[41] M. Yataghene, J. Legrand, A 3D-CFD model thermal analysis within a scraped surface heat exchanger, Comput. Fluids 71 (2013) 380–399.
[42] M. Yataghene, J. Pruvost, F. Fayolle, J. Legrand, CFD analysis of the flow pattern and local shear rate in a scraped surface heat exchanger, Chem. Eng. Process. Process Intensif. 47 (2008) 1550–1561.
[43] C. Diel, R. Canevesi, D. Zempulski, J. Awadallak, C. Borba, F. Palú, E. Silva, Optimization of multiple-effect evaporation in the pulp and paper industry using response surface methodology, Appl. Therm. Eng. 95 (2016) 18–23.
[44] V.B. Silva, A. Rouboa, Optimizing the DMFC operating conditions using a response surface method, Appl. Math. Comput. 218 (2012) 6733–6743.
[45] R.H. Myers, D.C. Montgomery, C.M. Anderson-Cook, Response surface methodology: process and product optimization using designed experiments, John Wiley & Sons, 2016.
[46] A. Malakizadi, S. Cedergren, I. Sadik, L. Nyborg, Inverse identification of flow stress in metal cutting process using Response Surface Methodology, Simul. Model. Pract. Theory 60 (2016) 40–53.
[47] S. Rashidi, M. Bovand, J.A. Esfahani, Optimization of partitioning inside a single slope solar still for performance improvement, Desalination 395 (2016) 79–91.
[48] M. Bovand, S. Rashidi, J.A. Esfahani, Optimum interaction between magnetohydrodynamics and nanofluid for thermal and drag management, J. Thermophys Heat Transfer 31 (2017) 218–229.
[49] S. Rashidi, M. Bovand, J.A. Esfahani, Structural optimization of nanofluid flow around an equilateral triangular obstacle, Energy 88 (2015) 385–398.
[51] S. Vahedi, A.Z. Ghadi, M. Valipour, Application of response surface methodology in the optimization of magneto-hydrodynamic flow around and through a porous circular cylinder, J. Mech. 34 (2018) 695–710.